Three Roads to Islet Bursting: Emergent Oscillations in Coupled Phantom Bursters

Charles L. Zimliki,*†‡ David Mears,† and Arthur Sherman*
*National Institutes of Health, Laboratory of Biological Modeling, Bethesda, Maryland; †Uniformed Services University of the Health Sciences, Department of Anatomy, Physiology and Genetics, Bethesda, Maryland; and ‡Johns Hopkins University, Department of Biomedical Engineering, Baltimore, Maryland

ABSTRACT Glucose-induced membrane potential and Ca^{2+} oscillations in isolated pancreatic β-cells occur over a wide range of frequencies, from >6/min (fast) to <1/min (slow). However, cells within intact islets generally oscillate with periods of 10–60 s (medium). The phantom bursting concept addresses how β-cells can generate such a wide range of frequencies. Here, we explore an updated phantom bursting model to determine how heterogeneity in a single parameter can explain both the broad frequency range observed in single cells and the rarity of medium oscillations. We then incorporate the single-cell model into an islet model with parameter heterogeneity. We show that strongly coupled islets must be composed of predominantly medium oscillating single cells or a mixture of fast and slow cells to robustly produce medium oscillations. Surprisingly, we find that this constraint does not hold for moderate coupling, and that robustly medium oscillating islets can arise from populations of single cells that are essentially all slow or all fast. Thus, with coupled phantom bursters, medium oscillating islets can be constructed out of cells that are either all fast, all slow, or a combination of the two.

INTRODUCTION

Pancreatic β-cells are found within micro-organs called islets of Langerhans. These cells are responsible for maintaining blood glucose homeostasis by secreting insulin through a stimulus-secretion coupling mechanism. A key step in glucose-induced insulin secretion is the generation of bursting electrical activity, which consists of alternating depolarized and hyperpolarized phases. Calcium-dependent action potentials during the depolarized active phases drive simultaneous oscillations of cytosolic calcium (Santos et al., 1991) and insulin release (Gilon et al., 1993).

A striking feature of glucose-induced bursting electrical activity is the wide range of periods over which the oscillations can occur. These oscillations can be classified based on period as fast (<10 s), medium (10–60 s) or slow (>60 s) (Bertram et al., 2000). Interestingly, medium oscillations appear to be an emergent property of β-cells within intact islets of Langerhans. Specifically, Atwater and colleagues found that 95% of islets exposed to 11 mM glucose oscillate in the medium regime (Atwater et al., 1989), whereas Bertram et al. (2000) showed that only 6% of isolated β-cells oscillated in this range. The majority of single β-cells exposed to glucose exhibit fast membrane potential bursts or continuous spiking activity (Bertram et al., 2000; Falke et al., 1989; Gopel et al., 1999b; Kinard et al., 1999; Zhang et al., 2003) with much slower oscillations occasionally being reported (Bertram et al., 2000; Larsson et al., 1996; Smith et al., 1990). Intracellular calcium oscillations measured from single β-cells and small clusters are typically in the slow regime (Dryselius et al., 1999; Gilon et al., 1994; Gylfe et al., 1998; Hellman et al., 1992; Henquin et al., 1998; Jonkers and Henquin, 2001; Jonkers et al., 1999; Lenzen et al., 2000; Liu et al., 1996, 1998), although fast oscillations have also been reported (Zhang et al., 2003).

The differences in behavior between single cells and islets have motivated theoretical analysis of potential underlying mechanisms. Smolen et al. (1993) showed that heterogeneity of model parameters resulted in single cells that were predominantly either silent or continuously active, with very few exhibiting medium bursting. When the cells were coupled, they synchronized into medium oscillations (Smolen et al., 1993). Another strategy introduced stochastic channel noise into a model (Atwater et al., 1983; Chay and Kang, 1988; Sherman and Rinzel, 1991). The noise disrupted the burst pattern in single cells, converting it to a fast pattern or continuous spiking. All of these studies used models with a single slow negative feedback process and were designed to produce medium bursts. Coupling acted to reduce the effects of noise or heterogeneity such that the medium pattern emerged. Therefore, these models were not able to replicate the wide range of burst frequencies that have been observed in isolated β-cells and islets.

The first models to produce fast, medium, and slow oscillations were developed by Chay (1996, 1997). In those models, the oscillations are primarily driven by the combined negative feedback effects of cytosolic and endoplasmic reticulum calcium concentration on calcium-dependent ion channels. Here we use a model that incorporates those same mechanisms as well as negative effects of calcium on the ATP/ADP ratio (Bertram and Sherman, 2004). This model is

Submitted December 12, 2003, and accepted for publication March 31, 2004.

Address reprint requests to Dr. Arthur Sherman, National Institutes of Health, National Institute of Diabetes and Digestive and Kidney Diseases, Laboratory of Biological Modeling, Building 12A, Rm. 4007, 12 South Dr. MSC 5621, Bethesda, MD 20892-5621. Tel.: 301-496-4325; Fax: 301-402-0535; E-mail: asherman@nih.gov

0006-3495/04/07/193/14 $2.00

doi: 10.1529/biophysj.103.038471

an updated version of the phantom bursting model (PBM), which generates fast, medium, and slow oscillations, without need of any biophysical process that operates on the medium timescale (Bertram et al., 2000). In the PBM, two processes (S1 and S2) are hypothesized to drive the fast and slow oscillations respectively. S1 and S2 have time constants of 1 s and 2 min respectively and activate hyperpolarizing currents, I_{S1} and I_{S2}. The burst is terminated when the sum of I_{S1} and I_{S2} reaches a certain threshold, and burst period is inversely related to the rate at which the threshold is achieved. The interaction of I_{S1} and I_{S2}, with neither current dominating, underlies medium bursting, hence the term phantom bursting.

Bertram and colleagues (2000) proposed that islets of Langerhans might be composed of cells that are inherently fast or slow, with medium oscillations resulting from electrical coupling of the cells. Although a two-cell model supported this proposal, the potential biophysical basis for the existence of primarily fast and primarily slow β-cells was not explored, nor were the effects of coupling in larger islet models.

In this article, we use the updated PBM to explore how parameter heterogeneity and cell-to-cell electrical coupling affect the oscillatory behavior of populations of single cells and islets. We go beyond previous heterogeneity studies by considering not just particular examples of isolated cell and population behavior but comprehensive histograms of behavior obtained under various assumptions. We show that by randomly distributing a single parameter within an islet via a unimodal distribution, we can produce single cells that oscillate over a wide range of frequencies that is predominantly weighted in the fast and slow regimes. As expected, electrical coupling among the fast and slow cells results in islets that exhibit medium oscillations. However, we also find that the complex effects of cell-to-cell coupling among phantom bursters allow populations of β-cells that are predominantly fast or predominantly slow to oscillate in the medium regime. We thus arrive at three distinct ways of combining single-cell properties to produce islet-like oscillations, which covers all the scenarios observed in experiments by various laboratories.

METHODS

The single-cell calcium-based phantom bursting model

The model used in this study is an updated version of the PBM described by Bertram et al. (2000). Bursting is driven by the interaction of three processes, which influence the calcium-sensitive or ATP-sensitive potassium channels. These processes are cytosolic calcium, endoplasmic reticulum calcium, and the adenosine nucleotide ratio (ADP/ATP). Although other currents have been proposed to participate in bursting, the model as constructed is consistent with reports of a slowly activating, calcium-sensitive potassium current in β-cells (Goforth et al., 2002; Gopel et al., 1999b), and the later discovery that ATP-sensitive potassium channels contribute a variable portion to this current (Kanno et al., 2002). A detailed description of the roles of each process in producing fast, medium, and slow bursts is given elsewhere (Bertram and Sherman, 2004). Briefly, fast oscillations are driven by the influence of cytosolic calcium on the calcium-sensitive potassium channel. Slow oscillations are driven by a combination of the effects of adenosine nucleotide ratio on the $K_{(ATP)}$ channel and the slow underlying influence of endoplasmic reticulum calcium on the cytosolic calcium. The equations are:

$$C_m\frac{dV}{dt} = -(I_{K(Ca)} + I_{K(ATP)} + I_{Ca} + I_K) \tag{1}$$

$$\frac{dn}{dt} = \frac{n_\infty(V) - n}{\tau_n} \tag{2}$$

$$\frac{dc}{dt} = f_{cyt}\{J_{mem} + J_{ER}\} \tag{3}$$

$$\frac{da}{dt} = \frac{a_\infty(c) - a}{\tau_a} \tag{4}$$

$$\frac{dc_{ER}}{dt} = -f_{ER}\left(\frac{V_{cyt}}{V_{ER}}\right)J_{ER}, \tag{5}$$

where V is the membrane potential, n is the open fraction of voltage-gated potassium channels, c is cytosolic free calcium, a is the normalized adenosine nucleotide ratio (ADP/ATP), and c_{ER} is endoplasmic reticulum free calcium.

The time course of voltage (V) is determined by the balance of membrane currents (Eq. 1), which include a calcium-sensitive potassium current ($I_{K(Ca)}$), a nucleotide-sensitive potassium current ($I_{K(ATP)}$), a voltage-dependent calcium current (I_{Ca}), and a delayed rectifier potassium current (I_K). The equations describing the currents are:

$$I_{K(Ca)} = g_{K(Ca)}\frac{c^5}{c^5 + k_D^5}(V - V_K) \tag{6}$$

$$I_{K(ATP)} = g_{K(ATP)}a(V - V_K) \tag{7}$$

$$I_K = g_K n(V - V_K) \tag{8}$$

$$I_{Ca} = g_{Ca}m_\infty(V)(V - V_{Ca}). \tag{9}$$

The fraction of open $K_{(ATP)}$ channels is given by a, the normalized ratio of ADP/ATP. Equation 10 describes the equilibrium function of the nucleotide ratio, (a_∞):

$$a_\infty(c) = \frac{1}{\left[1 + \exp\left\{\frac{R - c}{s_a}\right\}\right]}. \tag{10}$$

R is the calcium concentration at which the equilibrium function is half-maximal and is a modified version of the glucose sensing parameter described previously (Keizer and Magnus, 1989; Smolen et al., 1993).

The fast subsystem responsible for the action potential firing in this model is described by the delayed rectifier potassium current (I_K), Eq. 8 and the voltage-dependent calcium current (I_{Ca}), Eq. 9. The parameter values for these currents were based on experiments performed in isolated pancreatic β-cells (Rorsman and Trube, 1986) as in the initial version of this model (Bertram and Sherman, 2004). The delayed rectifier potassium current (I_K)

given by Eq. 8 has an activation component n (Eq. 4), which defines the fraction of open channels. The sigmoidal activation curve of this current is described by

$$n_\infty(V) = \frac{1}{\left[1 + \exp\left\{\frac{v_n - V}{s_n}\right\}\right]}. \quad (11)$$

The voltage-dependent calcium current (I_{Ca}) in Eq. 9 is assumed to activate instantaneously, with the activation function described by

$$m_\infty(V) = \frac{1}{\left[1 + \exp\left\{\frac{v_m - V}{s_m}\right\}\right]}. \quad (12)$$

The net cytosolic calcium flux in Eq. 3 consists of two components, representing calcium flux across the plasma membrane (J_{mem}, Eq. 13) and across the endoplasmic reticulum membrane (J_{ER}, Eq. 14):

$$J_{mem} = -(\alpha I_{Ca} + k_{PMCA} c) \quad (13)$$

$$J_{ER} = p_{leak}(c_{ER} - c) - k_{SERCA} c. \quad (14)$$

Parameters for calcium handling and metabolism are not well constrained by experiment and were chosen to achieve values for c, c_{er}, and a within representative ranges in the literature. Table 1 is a listing of parameters that were used to solve the set of differential equations. All parameters are fixed to these values unless otherwise stated in the figure caption.

Construction of the theoretical islet

Model islets were constructed of 125 cells in a 5 × 5 × 5 cubic lattice. Each cell was electrically connected to its nearest neighbor by the addition of a coupling current ($I_{coupl,j}$, Eq. 16) into the voltage equation (Eq. 15) of every cell:

$$C_m \frac{dV_j}{dt} = -(I_{K(Ca)} + I_{K(ATP)} + I_{Ca} + I_K + I_{coupl,j}) \quad (15)$$

$$I_{coupl,j} = g_c \sum_{i}^{neighbor_j} (V_j - V_i). \quad (16)$$

$I_{coupl,j}$ is the whole-cell coupling current for cell j, g_c is the electrical coupling conductance between cell j and each of its neighbors i. V_j is the membrane potential of cell j and V_i is the membrane potential of the nearest neighbors (i) of cell j. The number of neighbors surrounding cell j depends upon the position of cell j within the lattice, with internal, face, edge, and corner cells having six, five, four, and three nearest neighbors, respectively.

Note that we have not included diffusion of Ca^{2+} between cells. Simulations (not shown) incorporating this process indicate that unless it dominates direct electrical coupling, the effect on islet behavior is only quantitative, not qualitative. On the other hand, if Ca^{2+} diffusion is dominant, it cannot by itself synchronize islets, but rather prevents synchrony. Since this is not observed experimentally, we conclude that Ca^{2+} diffusion through gap junctions is not a significant factor and neglect it in the simulations that follow.

Distribution of $g_{K(Ca)}$ values in the theoretical islet

Cells were made heterogeneous by randomly distributing the $g_{K(Ca)}$ values within the islet using the Box-Mueller algorithm (Press et al., 1992). The number generated by the algorithm was transformed to a parameter distribution having population mean (μ) and standard deviation (σ). Negative conductance values were discarded and a new one was generated, resulting in a truncated Gaussian distribution of $g_{K(Ca)}$ in the model islets. All other parameter values within the islet were identical from cell-to-cell, with values shown in Table 1.

TABLE 1 Default parameter values used in the calcium-based phantom bursting model

Symbol	Description	Value
$g_{K(Ca)}$	Ca-sensitive K^+ conductance	Variable 0–1400 pS
$g_{K(ATP)}$	ATP-sensitive K^+ conductance	450 pS
g_K	Delayed rectifier K^+ conductance	3000 pS
g_{Ca}	Voltage-dependent Ca^{2+} conductance	1200 pS
V_K	K^+ reversal potential	−75 mV
V_{Ca}	Ca^{2+} reversal potential	25 mV
k_D	Ca^{2+} dissociation constant of the KCa channel	0.25 μM
τ_n	Activation time constant of the delayed rectifier K^+ channel	16 ms
τ_a	Adenosine nucleotide ratio time constant	300,000 ms
C_m	Membrane capacitance	5300 fF
R	Glucose sensing parameter	0.09 μM
s_a	Activation range of the nucleotide ratio	0.2 μM
f_{cyt}	Ratio of free to bound Ca^{2+} in cytosol	0.01
V_{cyt}/V_{ER}	Volumetric fraction of cytosol to ER	50
f_{ER}	Ratio of free to bound Ca^{2+} in ER	0.01
p_{leak}	Leak permeability constant in ER	4×10^{-5} ms^{-1}
k_{SERCA}	Rate constant of sarcoendoplasmic reticulum Ca^{2+} ATPase	0.2 ms^{-1}
k_{PMCA}	Rate constant of plasma membrane Ca^{2+} ATPase	0.1 ms^{-1}
α	Conversion factor: current to flux	2.25×10^{-6} μM/(ms × fA)
v_n	Half-maximal activation of delayed rectifier K^+ channel	−16 mV
s_n	Activation range of delayed rectifier K^+ channel	5.6 mV
v_m	Half-maximal activation of voltage dependent Ca^{2+} channel	−20 mV
s_m	Activation range of voltage dependent Ca^{2+} channel	12 mV
g_c	Cell-to-cell coupling conductance	0–900 pS

Numerical methods and steady-state analysis

An adaptive step size Runge-Kutta Fehlberg method was written in FORTRAN to solve the system of ordinary differential equations in the single-cell and islet cases. Computations were performed on the Biowulf cluster (http://biowulf.nih.gov/) at the National Institutes of Health. Computation time for one islet was ~1.5 h.

The time course of the oscillations was analyzed during the final 2000 s of a 4100 s simulation to ensure that steady state had been reached. A voltage threshold ($V_{thresh} = -58.5$ mV) was used to distinguish the active phase from silent phase for each cell. Islet average values for active phase duration, silent phase duration, burst period, and plateau fraction were determined by averaging the single cell values.

RESULTS

Single-cell burst periods with the calcium-based phantom bursting model

Fig. 1 shows the range of burst periods that can be obtained in the calcium-based phantom bursting model (cPBM) by varying the maximal conductance ($g_{K(Ca)}$) of the KCa current ($I_{K(Ca)}$). Changing the conductance modifies the sensitivity of $I_{K(Ca)}$ to calcium, providing less or more hyperpolarizing current for a given calcium level. When the value of $g_{K(Ca)}$ is set to 800 pS (Fig. 1 *A*), changes in $I_{K(Ca)}$ due to cytosolic calcium oscillations are sufficient to drive membrane potential oscillations with a burst period of 4.5 s. As seen in Fig. 1 *A*, the adenosine nucleotide ratio and endoplasmic reticulum (ER) calcium remain essentially constant during the burst. When we reduce the $g_{K(Ca)}$ value to low levels ($g_{K(Ca)} = 400$ pS, Fig. 1 *B*), the hyperpolarizing influence of $I_{K(Ca)}$ is insufficient to drive the burst pattern, and additional hyperpolarizing current is necessary to terminate the burst. This is provided by oscillations of the nucleotide ratio and ER calcium. An increase in the ratio of ADP to ATP enhances hyperpolarizing current through the $K_{(ATP)}$ channel and elevated ER calcium provides hyperpolarizing influence indirectly by increasing cytosolic calcium to activate additional $I_{K(Ca)}$. The burst terminates when the combined hyperpolarizing influence of these effects reaches threshold. Importantly, because the nucleotide ratio and ER dynamics are slow, the membrane potential oscillations are slow (burst period $T_b = 136$ s). An intermediate value of $g_{K(Ca)}$ (610 pS, Fig. 1 *C*) allows both $I_{K(Ca)}$ and $I_{K(ATP)}$ to provide hyperpolarizing current contributions to the membrane potential, and an intermediate oscillation emerges ($T_b = 28.5$ s). The intermediate bursting pattern is therefore a merging of mechanisms that are faster and much slower than the timescale of the burst.

The single-cell period-parameter relationship

To formally investigate the relationship between $g_{K(Ca)}$ and burst period, simulations were performed with $g_{K(Ca)}$ values ranging from 0 to 1400 pS. The corresponding period-parameter relationship is shown in Fig. 2 (*red*). Fast oscillations ($T_b < 10$ s) are found at $g_{K(Ca)}$ values >630 pS and slow oscillations ($T_b > 60$ s) are found at $g_{K(Ca)}$ values <555 pS. The steep transition from the fast to the slow bursting regimes results in a narrow range of $g_{K(Ca)}$ values (75 pS span) that produce medium oscillations (highlighted in *gray*). This narrow transition suggests that with natural cell-to-cell variation in $g_{K(Ca)}$, the probability of a cell having a $g_{K(Ca)}$ value that results in medium oscillations could be small.

To further explore this possibility, we calculated the probability of finding fast, medium, and slow cells for various Gaussian distributions of $g_{K(Ca)}$. We first examined the effect of narrow distributions ($\sigma = 25$ pS; Fig. 2, *curves A–C*). These distributions can create a high probability of finding single cells that oscillate either in the slow (*curve A*, $\mu = 300$ pS, 100% slow), medium (*curve B*, $\mu = 600$ pS, 82.9% medium), or fast (*curve C*, $\mu = 900$ pS, 100% fast) regime. With a broader $g_{K(Ca)}$ distribution (*curve D*, $\sigma = 300$ pS, $\mu = 400$ pS), the probability of finding single cell oscillations is heavily weighted in the fast and slow regimes (67.3% slow, 8.3% medium, and 24.4% fast). Although it is evident that one can obtain populations of fast and slow oscillating cells with a bimodal $g_{K(Ca)}$ distribution, curve *D* shows that it is also possible to obtain a bimodal appearance with a unimodal distribution of $g_{K(Ca)}$ values. We will show next that, in addition to the narrow transition through the medium regime, the step or notch in the period-parameter

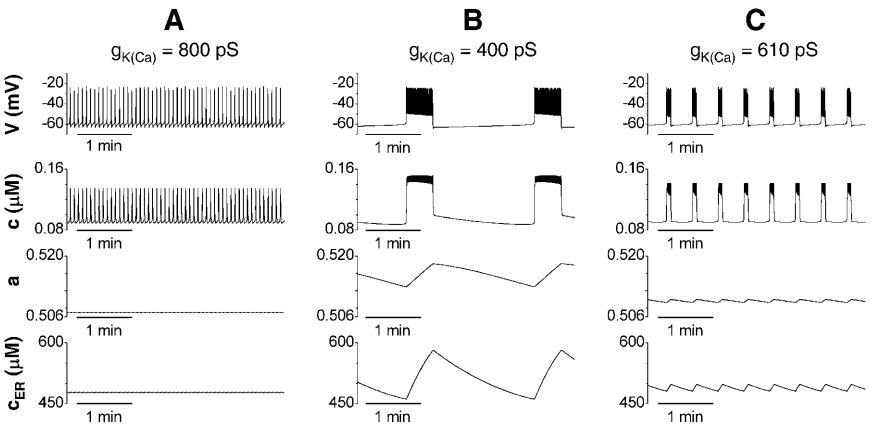

FIGURE 1 Oscillations in the calcium-based phantom bursting model. Time course of oscillations in the cPBM for various oscillation frequencies. Membrane potential (V), cytosolic calcium (c), adenosine nucleotide ratio ADP/ATP (a), and endoplasmic reticulum calcium (c_{ER}) are shown. Changing the value of the $g_{K(Ca)}$ parameter alters burst period. (*A*) $g_{K(Ca)} = 800$ pS; fast oscillations occur when the rise and fall of cytosolic calcium can terminate the burst via $I_{K(Ca)}$. (*B*) $g_{K(Ca)} = 400$ pS; slow oscillations occur when the cytosolic calcium oscillations are insufficient to terminate the burst and additional current from $I_{K(ATP)}$ (i.e., a and its inherent slow dynamics) is necessary to drive the burst pattern. (*C*) $g_{K(Ca)} = 610$ pS, medium oscillations occur when current from both $I_{K(Ca)}$ and $I_{K(ATP)}$ are necessary to terminate the burst.

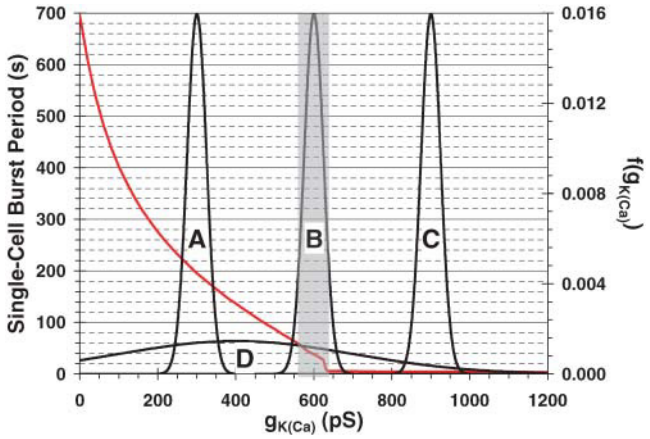

FIGURE 2 Single-cell period-parameter ($g_{K(Ca)}$) relationship. Single-cell burst period for various $g_{K(Ca)}$ values (*red line*). Increasing $g_{K(Ca)}$ results in a steadily decreasing burst period with a sharp transition through the medium regime (highlighted in *gray*; $g_{K(Ca)} \approx 550$–635 pS). Fast oscillations occur once $g_{K(Ca)}$ is large enough to terminate the burst and burst period gradually decreases as $g_{K(Ca)}$ increases. Four $g_{K(Ca)}$ density functions (*right axis*) are shown in black and labeled *A–D*. When the distribution of $g_{K(Ca)}$ is narrow ($\sigma = 25$ pS, curves *A–C*), we can create a high probability of finding single cells that oscillate in either the slow (*curve A*, $\mu = 300$ pS, 100% slow), medium (*curve B*, $\mu = 600$ pS, 82.9% medium), or fast (*curve C*, $\mu = 900$ pS, 100% fast) regime. Broadening the distribution (*curve D*, $\sigma = 300$ pS, $\mu = 400$ pS) can produce a distribution of $g_{K(Ca)}$ values that are heavily weighted in the fast and slow oscillating regimes (67.3% slow, 8.3% medium, and 24.4% fast).

relationship just above 600 pS also contributes significantly to the bimodality of the period distribution.

Calculation of the single-cell period density function

Fig. 3 demonstrates the mathematical basis for the bimodal period distribution obtained with curve *D* in Fig. 2. Given a single-cell period-parameter relationship (ϕ) that monotonically decreases (Fig. 2, *red*), and a $g_{K(Ca)}$ density function (f), we can use the change of variable formula (Hoel et al., 1971) to calculate the period density function and hence the probability of finding oscillating single cells in the fast, medium, and slow regimes. The period-parameter relationship shown in Fig. 2 (*red*) is symbolized as

$$T_b = \phi(g_{K(Ca)}). \tag{17}$$

Density function f is a nonnegative function whose integral from $-\infty$ to $+\infty$ is equal to 1. Since our density function is truncated, we renormalize it such that the integral of f from 0 to $+\infty$ is equal to 1. Given these two functions, we can proceed to calculate the single-cell period density function by Eq. 18:

$$g(g_{K(Ca)}) = \frac{f(g_{K(Ca)})}{\left| dT_b \Big/ dg_{K(Ca)} \right|} = \frac{f(g_{K(Ca)})}{|\phi'(g_{K(Ca)})|}. \tag{18}$$

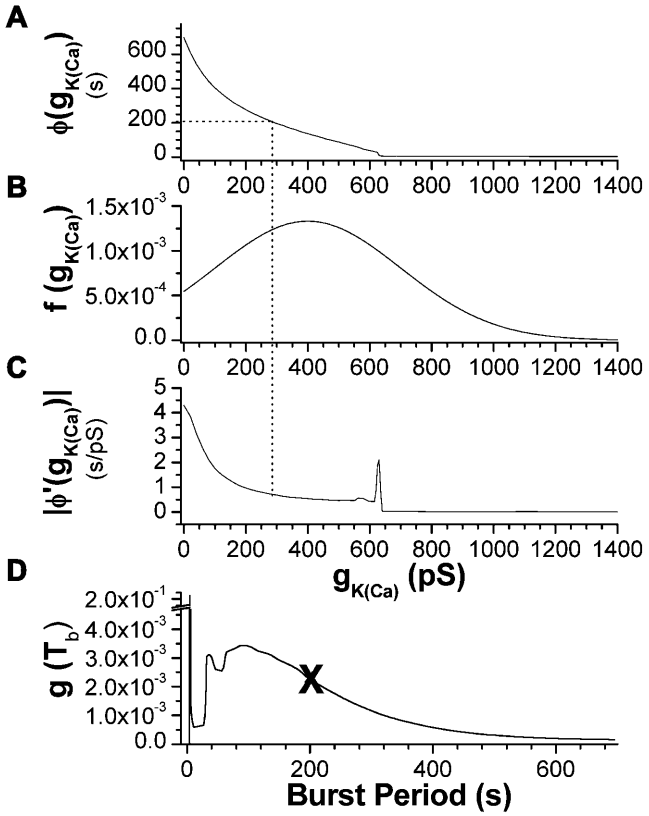

FIGURE 3 Calculation of the period density function. Three graphs are necessary to calculate (*D*) the period density function $g(T_b)$: (*A*) the period-parameter relationship $\phi(g_{K(Ca)})$, (*B*) the density function $f(g_{K(Ca)})$ representing the $g_{K(Ca)}$ distribution (in this case $\mu = 400$ pS, $\sigma = 300$ pS), and (*C*) the absolute value of the derivative of the period-parameter relationship $|\phi'(g_{K(Ca)})|$. The dotted line represents a set of values that are needed to calculate a point for the specific density function $g(T_b)$. Equation 2 states that the value of $g(T_b)$ is the quotient of *B* over *C* at the burst period represented in *A*. The black *X* in *D* identifies the point calculated from the dotted line.

$g(g_{K(Ca)})$ is the desired density function of burst period with respect to the $g_{K(Ca)}$ parameter.

For Eq. 18 to be valid, the inverse ϕ^{-1} of the period-parameter relationship ϕ in Eq. 17 must provide a unique value of $g_{K(Ca)}$ for each value of T_b. This is guaranteed because ϕ is monotonic. Substituting Eq. 17 into 18 expresses the period density function $g(T_b)$ in terms of T_b:

$$g(T_b) = \frac{f(\phi^{-1}(T_b))}{|\phi'(\phi^{-1}(T_b))|}. \tag{19}$$

Equation 19 relates the period density distribution $g(T_b)$ to given or calculable relationships as described next.

Graphical calculation of single-cell period density function

Fig. 3 illustrates graphically the procedure for calculating the period density function $g(T_b)$ using Eq. 19. The single-cell

period-parameter relationship $\phi(g_{K(Ca)})$ from Fig. 2 (*red*) is replotted in Fig. 3 *A*. The $g_{K(Ca)}$ density function (f) is plotted in Fig. 3 *B* for the case $\mu = 400$ pS, $\sigma = 300$ pS, as in Fig. 2, curve *D*. The derivative of ϕ with respect to $g_{K(Ca)}$ was calculated numerically and plotted in Fig. 3 *C*. The inverse of ϕ, ϕ^{-1} (not shown), was linearly interpolated between the known points. With these four pieces of information, we can find any desired value for $g(T_b)$. We illustrate for $T_b = 200$ s (*black X* in Fig. 3 *D*). Starting with the value 200 s on the vertical axis of Fig. 3 *A*, we project to the right and down (*dotted lines*) to find the corresponding value of $g_{K(Ca)}$ and evaluate f and ϕ' for that value. The quotient (Eq. 19) gives the value of g. The resulting curve for g (Fig. 3 *D*) is bimodal, with a sharp peak in the fast regime ($T_b = 4.5$ s) and a broad peak in the slow regime ($T_b = 91.6$ s).

The large dip in the period distribution g in the medium range is due in part to the broad shape of f, which reduces the numerator in Eq. 19, but mainly to the peak in $|\phi'(g_{K(Ca)})|$ for $g_{K(Ca)}$ just above 600 pS (Fig. 3 *C*), which increases the denominator in Eq. 19. The peak in ϕ' in turn corresponds to the notch in ϕ (Fig. 3 *A*). Thus, the features of ϕ and f combine to create a minimum within the medium range of the period density function g.

To confirm the prediction of Fig. 3 *D*, we randomly distributed the $g_{K(Ca)}$ parameter value in the cPBM while keeping all other parameters fixed. The $g_{K(Ca)}$ values were randomly chosen for 125,000 cells using the $g_{K(Ca)}$ distribution with parameters $\mu = 400$ pS and $\sigma = 300$ pS. Fig. 4 *A* shows the histogram of the $g_{K(Ca)}$ values, and Fig. 4 *B* shows the histogram of the corresponding periods. As expected, the shapes of the $g_{K(Ca)}$ and single-cell period histograms closely match the shapes of the $g_{K(Ca)}$ and period density functions that were calculated in Fig. 3, *B* and *D* (superimposed as *solid lines* in Fig. 4, *A* and *B*). The percentages of fast, medium, and slow cells resulting from this $g_{K(Ca)}$ parameter distribution are 24.29, 8.62, and 67.09, respectively. (The small differences between these percentages and those for Fig. 2 reflect sampling error.) Together, Figs. 3 and 4 confirm that an increase in the slope of the period-parameter relationship in the medium regime can transform a unimodal parameter ($g_{K(Ca)}$) distribution into a single-cell period distribution that is composed of a heterogeneous mixture of primarily fast and slow oscillating cells. We next examine whether islets composed of such cells can show medium oscillations.

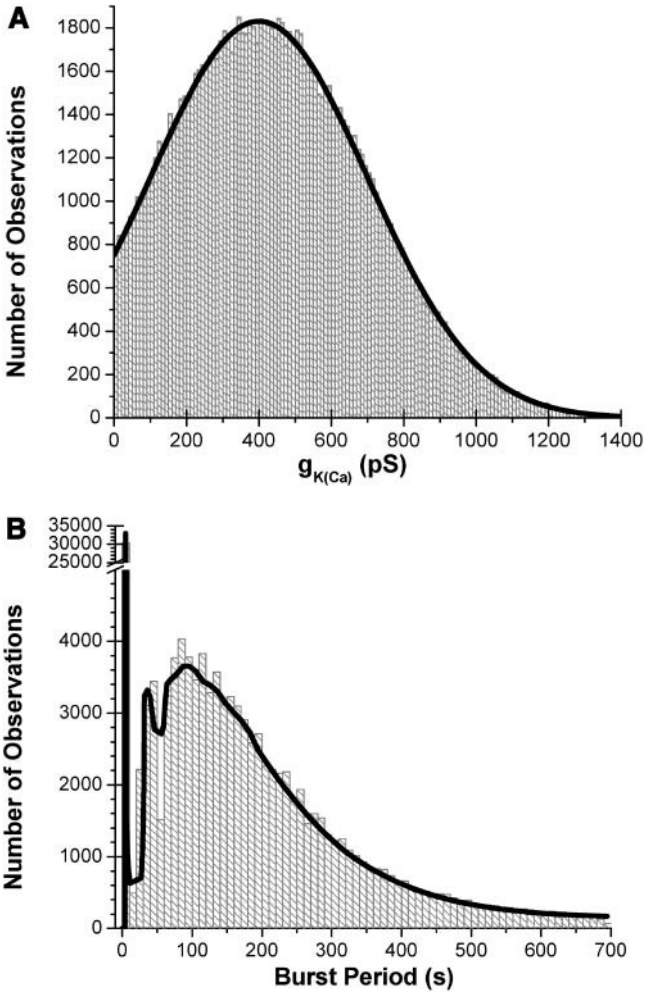

FIGURE 4 Single-cell $g_{K(Ca)}$ and burst period distribution. We constructed 125,000 cells according to the following $g_{K(Ca)}$ distribution: (*A*) $g_{K(Ca)}$ parameter distribution of single cells ($\mu = 400$ pS, $\sigma = 300$ pS). The resultant single-cell period distribution from the $g_{K(Ca)}$ parameter distribution in *A*. The population of single cells is 24.29% fast, 8.62% medium, and 67.09% slow. Superimposed on each graph in black is the density function $f(g_{K(Ca)})$ in *A* and the period density function $g(T_b)$ in *B*.

Extending the single-cell period density function to predict the islet period density function

Because the distributed parameter, $g_{K(Ca)}$, appears linearly in the equation for membrane potential (Eqs. 1 and 6), we can use the single-cell period density function to predict the islet behavior. The reason is that when the cells are very strongly coupled, the islet will behave like a single cell with the averaged parameter values of the islet (de Vries and Sherman, 2001). Therefore, the period-parameter relationship for strongly coupled islets is equal to the single-cell period-parameter relationship in Fig. 3 *A*, where $g_{K(Ca)}$ is the population average value for all cells in the islet. The density function $f_{islet}(g_{K(Ca)})$ is the distribution of the islet average $g_{K(Ca)}$ values, with mean (μ_{islet}) and standard deviation (σ_{islet}). For islets containing N cells, the standard deviation σ_{islet} is $\sigma/N^{1/2}$, where σ is the standard deviation of the single cell distribution. We can therefore simulate the decrease in islet-to-islet variability that accompanies increases in islet size by decreasing σ_{islet} in the density function, $f_{islet}(g_{K(Ca)})$. Fig. 5 illustrates the effect of increasing islet size by reducing σ_{islet} on the resulting islet period density function. Fig. 5 *A* corresponds to an ''islet'' of 1 cell with the same density f for $g_{K(Ca)}$ as in Fig. 3 *B*. Here, σ_{islet} equals σ for the single-cell

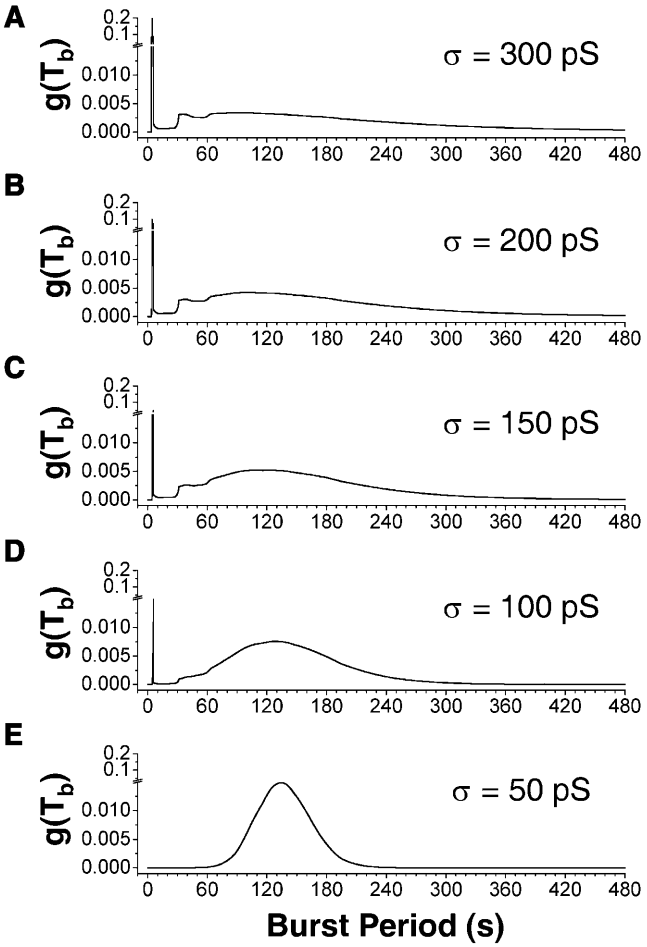

FIGURE 5 Approximation of the islet-period density function. The islet-period density function can be approximated by assuming that the islet period-parameter relationship $\phi(g_{K(Ca)})$ is the same as the single-cell period-parameter relationship in Fig. 3 *D*. If we keep the original single-cell period-parameter relationship, we can mimic the transformation of the single-cell period density function to the islet-period density function by reducing σ in the parameter density function. In *A*, $\sigma = 300$ pS, the period density function is similar to the single-cell density function calculated in Fig. 3 *D*. Reducing σ to values of *B*, $\sigma = 200$ pS; *C*, $\sigma = 150$ pS; *D*, $\sigma = 100$; and *E*, $\sigma = 50$ pS simulates the transformation of the single-cell parameter distribution into the distribution of islet-to-islet sample $g_{K(Ca)}$ means. When σ is decreased, the peaks in the fast and slow regimes converge.

$g_{K(Ca)}$ distribution, and the islet period density function is identical to the single-cell period density function in Fig. 3 *D*. As the islet-to-islet variability σ_{islet} is reduced, the two peaks of the bimodal period distribution converge. The result is a unimodal period islet distribution centered around the period corresponding to the population mean of $g_{K(Ca)} = 400$ pS, or a period of a little more than 2 min. Thus, not surprisingly, if we construct islets out of mostly slow cells and couple them strongly, the islet is slow.

Alternatively, suppose we take a broad single-cell $g_{K(Ca)}$ distribution like curve *D* in Fig. 2, but centered around $g_{K(Ca)} = 600$ pS (a value that produces medium bursting). If σ is large enough, the single-cell period distribution will be bimodal with mostly fast and slow cells, as was the case using curve *D*. However, in this case the islets will exhibit mostly medium bursting provided they contain sufficiently many cells and are sufficiently well-coupled. For strongly coupled islets, this is the only scenario that will result in medium bursting, aside from the trivial case of single cells that are medium bursters to begin with.

We next show that if we consider coupling that is not very strong, but moderate, it is possible to get medium islets even when the average cell is slow or fast. We do not have a theory to predict islet behavior from single-cell behavior for moderate coupling, so we have to carry out direct numerical simulations.

Effects of coupling on the $g_{K(Ca)}$-distributed islet

Previous studies using classical models with a single slow variable have shown that weak or moderate electrical coupling can result in burst periods that are longer than those of the average cell (Sherman and Rinzel, 1991). We therefore examine the effects of coupling on populations of heterogeneous phantom bursters. Islets were constructed in a $5 \times 5 \times 5$ cell lattice and their $g_{K(Ca)}$ values distributed according to a truncated Gaussian distribution as described in Methods. The average islet burst period was determined by averaging all of the single-cell burst periods from the 125 cells. Islets were defined to be synchronous if the standard deviation of the burst periods in the 125-cell islet was <500 ms.

Fig. 6 shows the effects of cell-to-cell coupling on islet burst period for one islet. The $g_{K(Ca)}$ values were randomly distributed among the 125 cells using a distribution with $\mu = 400$ and $\sigma = 300$ pS, the same distribution used to produce the burst period histogram shown in Fig. 4 *B*. The period of a single cell with the population average value of $g_{K(Ca)} = 440.7$ pS is shown by the gray line. The curve of islet period shows a maximum near $g_c = 100$ pS with burst periods longer than that of the average cell; this confirms that the period-lengthening effect previously described for classical models applies to phantom-type models as well. Note that at this relatively weak coupling the intraislet period variability is large, as indicated by the large error bars. Full synchrony is not achieved until approximately $g_c = 220$ pS. For values of g_c larger than $\sim$350 pS, there is a plateau region where the islet periods are a little longer than the single-cell period but converge to the single-cell period as g_c increases. This is the regime where the period distribution analysis of the previous section applies. Most interesting, however, is that the islet period curve has a minimum near $g_c = 320$ pS with burst periods shorter than the average cell. This phenomenon has not been previously observed in nonphantom models. Thus, at least for the example shown in Fig. 6, there exists a range of g_c values that produce medium bursting, despite the fact that a single cell having parameters equal to the islet average oscillates in the slow regime.

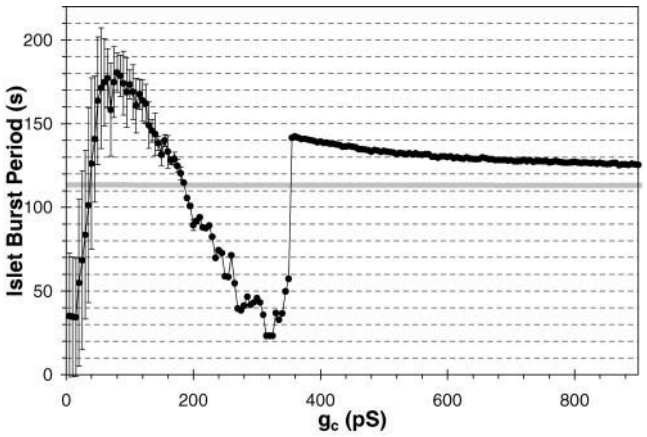

FIGURE 6 Effects of cell-to-cell coupling conductance on the average islet burst period. Each symbol represents the islet average burst period at a specific cell-to-cell conductance for a single islet with the same $g_{K(Ca)}$ distribution as curve *D*, Fig. 2 ($\mu = 400$ pS, $\sigma = 300$ pS). Error bars indicate variation in single cell oscillations within the islet. Synchronization (i.e., standard deviation of the averaged cells period <500 ms) occurs at a cell-to-cell coupling conductance of 220 pS. The shaded line identifies the single-cell period (114 s) of a single cell with the same $g_{K(Ca)}$ value as the islet average $g_{K(Ca)}$ value ($g_{K(Ca)} = 440.7$ pS). In this model, the islet period can be less than ($g_c = 190$–350 pS) or greater than ($g_c \geq 355$ pS) the single-cell period and maintain synchrony.

The mathematical basis for the interesting effects of diffuse coupling on heterogeneous phantom bursters is discussed below in the Discussion section. For now, we focus on the practical implications of Fig. 6. Fig. 7, *A–C*, shows the time courses of V, c, a, and c_{ER} of two cells within the $g_{K(Ca)}$-distributed islet of Fig. 6 at coupling conductances of 0, 300, and 360 pS. The time courses of a face cell are shown in black ($g_{K(Ca)} = 158.5$ pS) and those of an internal cell are shown in red ($g_{K(Ca)} = 890.1$ pS). With $g_c = 0$ pS (Fig. 7 *A*), each cell oscillates independently with burst period determined exclusively by its $g_{K(Ca)}$ value ($T_b = 319.4$ s and $T_b = 4.7$ s, respectively). As shown in Fig. 7 *B*, when the coupling conductance is increased to 360 pS (in the plateau region of Fig. 6), the cells in the islet oscillate synchronously in the slow regime ($T_b = 142.4$ s). Finally, at an intermediate coupling strength ($g_c = 300$ pS, in the valley of Fig. 6), the islet maintains its synchrony, but the burst period is reduced, falling within the medium regime (45.7 s, Fig. 7 *C*). We have thus found a single example of an islet in which the average cell is slow but the islet is medium. We next examine a population of islets with the same $g_{K(Ca)}$ distribution and coupling strength to assess whether this behavior is representative.

Finding robust islet oscillations in the $g_{K(Ca)}$-distributed islet

In light of experimental evidence that islet bursts have almost exclusively medium periods (Atwater et al., 1980), we now explore whether our values for μ, σ, and g_c in the islet model can robustly produce medium oscillations by simulating multiple islets. We use the same $g_{K(Ca)}$ distribution ($\mu = 400$ pS, $\sigma = 300$ pS) from which the islet in Figs. 6 and 7 was drawn to construct 1000 islets, each containing 125 cells and coupled with a g_c of 300 pS. Fig. 8 *A* shows the histogram of islet average $g_{K(Ca)}$values for the 1000 islets. Notice that this histogram is centered on a $g_{K(Ca)}$ value of 454 pS, which falls in the slow regime of the single-cell period-parameter relationship (Fig. 2). (The population mean is significantly larger than μ because of the truncation of the broad $g_{K(Ca)}$ distribution at 0.) The islet period histogram is shown in Fig. 8 *B*. The distribution of islet periods is 0.0% fast, 92.5% medium, and 7.5% slow. Combined, Figs. 4 and 8 demonstrate that unlike the case for strong coupling, the islet average $g_{K(Ca)}$ distribution need not be centered in the medium regime of the single-cell period-parameter relationship to robustly produce medium oscillations. We note that medium bursting still requires a relatively narrow range of values of g_c, but coupling of cells would likely also overcome heterogeneity in coupling conductance, as found in the simulations of Smolen et al. (1993).

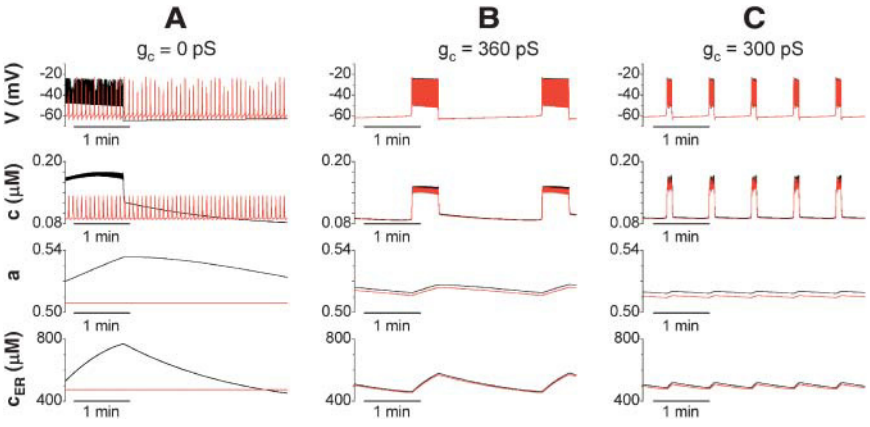

FIGURE 7 Effects of coupling on two cells within the $g_{K(Ca)}$-distributed islet. Islet $g_{K(Ca)}$ distribution ($\mu = 400$ pS, $\sigma = 300$ pS) with islet average $g_{K(Ca)} = 440.7$ pS. Two cells were selected for illustration: a face cell (*black*) $g_{K(Ca)} = 158.5$ pS, and an internal cell (*red*) $g_{K(Ca)} = 890.1$ pS. Coupling conductances of (*A*) 0 pS, (*B*) 360 pS, and (*C*) 300 pS are illustrated. At $g_c = 0$ pS, cells oscillate at their intrinsic burst periods, determined by their $g_{K(Ca)}$ values. Increasing g_c to 300 pS synchronizes the cells and results in an islet burst period in the medium regime ($T_b = 45.7$ s). A further increase in g_c to 360 pS maintains the synchronization but results in islet burst period in the slow regime ($T_b = 142.4$ s).

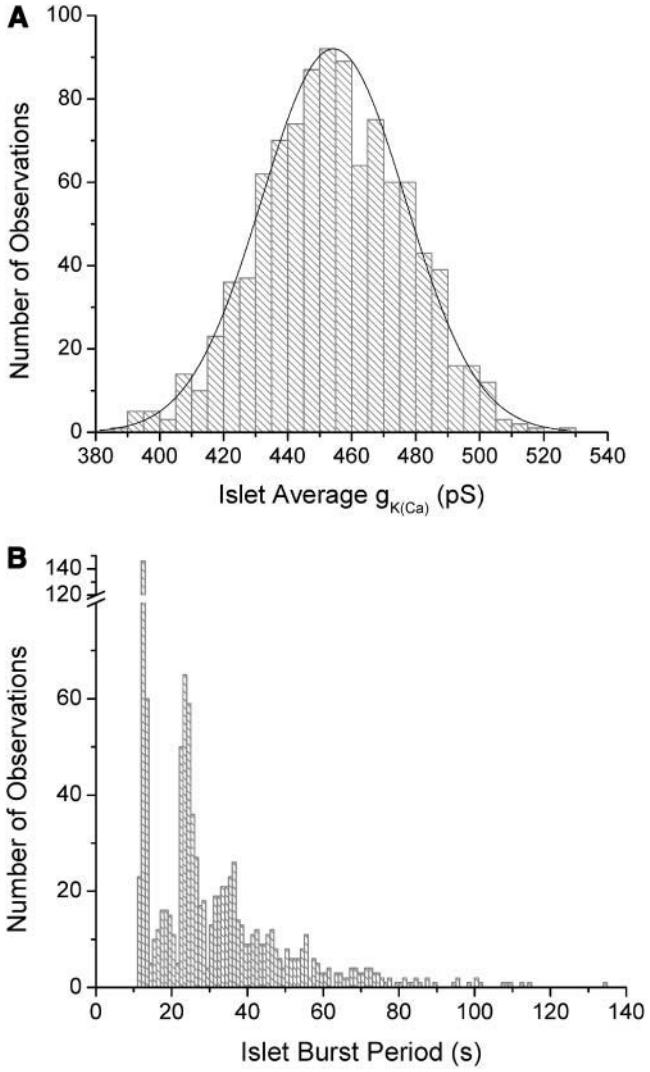

FIGURE 8 Islet average $g_{K(Ca)}$ and burst period distributions. We constructed 1,000 islets (125,000 cells) and simulated (using the single-cell $g_{K(Ca)}$ distribution of Fig. 4 *A*, $\mu = 400$ pS, $\sigma = 300$ pS, $g_c = 300$ pS). (*A*) Distribution of the islet sample means ($\mu = 454.3$ pS, $\sigma = 23.4$ pS, R^2 value = 0.976). The rightward shift of the islet sample means is associated with the truncation of the $g_{K(Ca)}$ parameter distribution. (*B*) Islet burst period distribution. Islet burst period identification: 0.0% fast, 92.5% medium, and 7.5% slow.

Medium oscillations from islet containing only slow or only fast cells with intermediate coupling

The results so far have shown two ways to construct medium-bursting islets out of cells whose intrinsic periods are bimodally distributed to be predominantly fast or slow. This was achieved with a natural, unimodal distribution of $g_{K(Ca)}$. Fig. 6, however, raises two additional possibilities. Depending on coupling strength, the period of the islet can be either faster or slower than that of a single cell with average properties. We therefore sought to extend the analysis of the preceding section to determine if medium oscillations could emerge robustly in islets that are composed of predominantly fast or predominantly slow single cells. The $g_{K(Ca)}$ values were distributed in model islets using various μ and σ values in the single-cell parameter distribution. Islet oscillations were then simulated for different values of g_c. Table 2 shows scenarios for which medium oscillations were robustly observed when the single-cell period distribution consisted of i), a mixture of fast and slow cells, ii), mostly slow cells, and iii), mostly fast cells. The first row is the example described previously with single-cell period distribution and islet period distribution shown in Figs. 4 *B* and 8 *B*, respectively. The single-cell period distributions and islet period distributions for the examples in rows two and three of Table 2 are shown in Fig. 9. In the case of row 2, 99.5% of the single cells exhibited slow oscillations, yet medium oscillations were observed in 92.7% of the islets. In the example of row 3, medium oscillations were observed in 90.5% of the islets, which were composed of 77.5% fast oscillating single cells. We note that these examples are best-case scenarios and that the robustness of medium-emergent-islet oscillations depends strongly on the choices of μ, σ, and g_c. Nevertheless, the results demonstrate that if these parameters are chosen correctly, predominantly medium-oscillating islets can be generated from a wide assortment of single-cell burst period distributions. In particular, islets coupled with intermediate strength, unlike strongly coupled islets, are not constrained to contain both slow and fast cells to oscillate in the medium regime. Together, our results demonstrate that the addition of parameter heterogeneity and diffuse coupling to the phantom bursting model could provide a theoretical explanation for the widely disparate oscillatory behavior between single β-cells and those within islets.

DISCUSSION

We have reexamined the question of why bursting oscillations with periods of tens of seconds are observed regularly in pancreatic islets, but rarely in isolated β-cells. Some laboratories have reported that isolated cells are an order of magnitude faster than islets (Falke et al., 1989; Kinard et al., 1999; Zhang et al., 2003), whereas others have reported that isolated cells are an order of magnitude slower than islets (Dryselius et al., 1999; Hellman et al., 1992; Jonkers and Henquin, 2001; Larsson et al., 1996; Smith et al., 1990). Here we have considered three possibilities—that islet behavior is the result of combining heterogeneous populations of fast and slow cells; the result of combining fast cells only; or the result of combining slow cells only.

We cannot rule out the possibility that the electrophysiological and calcium handling properties of isolated β-cells are fundamentally different from those within the three-dimensional architecture of the islet (Gopel et al., 1999a,b). Such differences could be brought about by paracrine secretions (Bertuzzi et al., 1999; Chay, 1997; Grapengiesser

TABLE 2 Table of various $g_{K(Ca)}$ parameter distributions and islet simulations

Single-cell $g_{K(Ca)}$ distribution						Islet distribution					
μ	σ	n (cells)	Fast %	Medium %	Slow %	g_c (pS)	n (islets)	Fast %	Medium %	Slow %	Synchronized islets (%)
400	300	125,000	24.29	8.62	67.09	300	1,000	0	92.5	7.5	100.0
430	50	125,000	0.004	0.493	99.503	270	1,000	0	92.7	7.3	99.9
785	200	125,000	77.51	9.64	12.84	140	1,000	9.5	90.5	0	97.3

et al., 1999; Liu et al., 1998; Squires et al., 2000), K^+ diffusion (Perez-Armendariz and Atwater, 1986; Perez-Armendariz et al., 1985), or the isolation procedure itself. In fact, Gopel et al. (1999b) have reported that the calcium-sensitive potassium current is reduced when β-cells are isolated from their islet configuration. In our model, a reduction in the single-cell K(Ca) current would tend to slow the single-cell oscillation (Fig. 2) and create populations of single cells biased toward the slow regime, other things being equal. However, we note that Goforth et al. (2002) did not find a significant difference in K(Ca) current between isolated cells and islets. In fact, induction of medium bursting in fast isolated cells by injection of small currents suggests that any such differences are modest and quantitative (Bertram et al., 2000; Zhang et al., 2003). Therefore, our goal here was to determine theoretically if the disparities in oscillatory behavior could be explained in the absence of such fundamental differences.

A previous study (Smolen et al., 1993) also considered heterogeneity as a source of the differences between islets and single cells. At that time, data on single-cell behavior were limited, and the early modeling effort assumed that the average cell was a medium burster, but that the population was diverse. The model predicted that most cells would be either silent or continuously spiking. More recent data on single cells indicate that they tend to be oscillatory (see below), but with either a much shorter or longer period than islets. We have therefore used a version of the phantom bursting model, which readily produces fast and slow cells. The key to this capability is the variable mixing of two or more slow variables with disparate time constants.

The particular version of the phantom bursting model used in this study is able to reproduce a number of in vitro experimental observations, including the triphasic intracellular Ca^{2+} response to glucose and the effects of SERCA inhibitors on medium and slow bursting (Bertram and Sherman, 2004). However, the analysis here is not intended to justify this particular biophysical implementation of the model, but rather to determine if cell-to-cell electrical coupling among heterogeneous cells with phantom burst

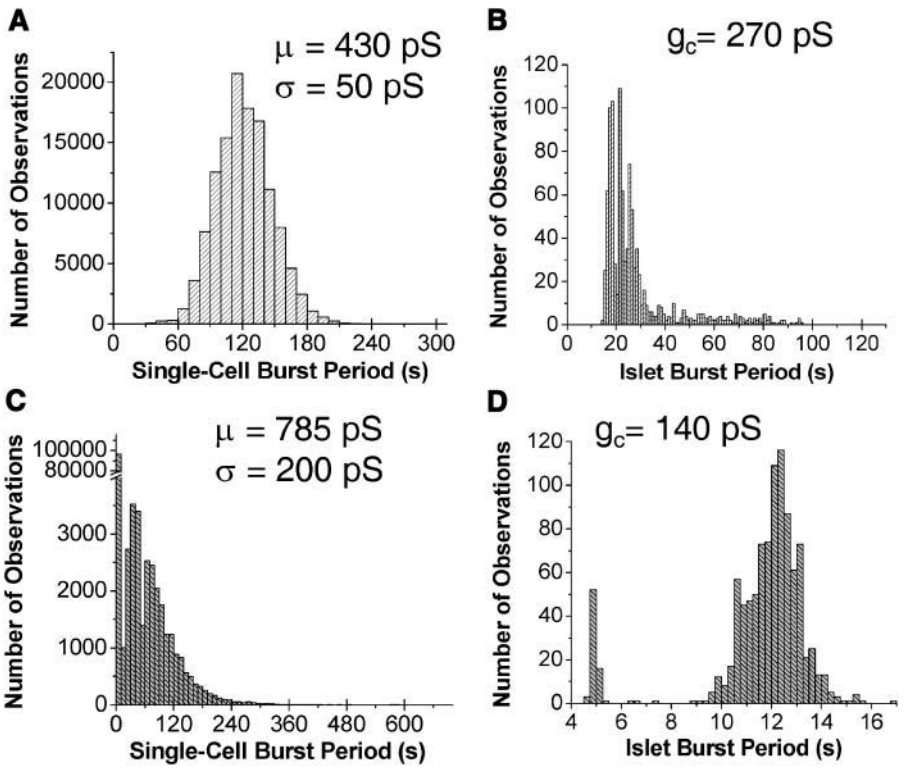

FIGURE 9 Single-cell and islet burst period distributions for selected $g_{K(Ca)}$ distributions. Two $g_{K(Ca)}$ distributions of 1,000 islets (125,000 cells) were constructed and simulated. The first $g_{K(Ca)}$ distribution shown ($\mu = 430$ pS, $\sigma = 50$ pS) results in the single-cell period distribution (*A*) with single-cell period identification: 0.004% fast, 0.493% medium, and 99.503% slow. When the islets of this specific distribution are coupled ($g_c = 270$ pS), the resultant islet period distribution in *B* occurs with islet identification: 0.0% fast, 92.7% medium, and 7.3% slow. The second $g_{K(Ca)}$ distribution shown ($\mu = 785$ pS, $\sigma = 200$ pS) results in the single-cell period distribution (*C*) with single-cell period identification: 77.51% fast, 9.64% medium, and 12.84% slow. When the islets of this specific distribution are coupled ($g_c = 140$ pS), the resultant islet period distribution in *D* occurs with islet identification: 9.5% fast, 90.5% medium, and 0.0% slow.

capabilities can provide a theoretical explanation for the experimentally observed disparity between single-cell and whole-islet oscillatory behavior. In fact, we arrived at the same conclusions using a phantom burst model with two generic slow variables and no ER (Zimliki, 2001).

Bertram et al. (2000) had shown with the earlier version of the phantom burst model that coupling fast and slow cells could result in medium bursting, but this left open the question of how to construct islets with a bimodal distribution of burst periods in a natural way. Study of this question also gave insight into how to make medium islets using exclusively fast or slow cells.

One conceptually simple way to alter the burst period in a phantom bursting model is to change the whole-cell conductance of the current associated with the fastest slow variable, in this case $g_{K(Ca)}$. Our analysis of the relationship between $g_{K(Ca)}$ and single-cell burst period over a broad range of $g_{K(Ca)}$ showed that the burst period decreases monotonically with the parameter value. Importantly, we found that medium bursting is observed only for a very restricted range of $g_{K(Ca)}$ values (Fig. 2, *red curve*). This feature is amplified by a sharp transition from slow to fast bursting as $g_{K(Ca)}$ increases, which further drives down the probability of obtaining medium-bursting cells. The result indicates that for a population of single β-cells to exhibit predominantly medium bursting, very little cell-to-cell heterogeneity in $g_{K(Ca)}$ can be tolerated, such that most $g_{K(Ca)}$ values will fall into this restricted range. The fact that medium oscillating single cells are rarely observed experimentally suggests that such a tight clustering of $g_{K(Ca)}$ values is not an appropriate model for β-cells.

We next examined how a natural, unimodal distribution of $g_{K(Ca)}$ values affects the bursting behavior of a population of β-cells. In the absence of experimental measurements of the distribution of this parameter in β-cells, we chose Gaussian distributions, which are mathematically simple and ubiquitous in biology. As expected, most cells in a given population behave similarly when the standard deviation of the $g_{K(Ca)}$ distribution is small, resulting in essentially all fast, all medium, or all slow cells, depending on the mean value of $g_{K(Ca)}$ (Fig. 2, *curves A*, *B*, and *C*). However, when the standard deviation is larger, the unimodal distribution of single-cell $g_{K(Ca)}$ values (Fig. 2, *curve D*; Fig. 4) can produce a bimodal distribution of single-cell burst periods (Fig. 4 *B*). The population then consists predominantly of fast and slow single cells, with relatively few medium bursters. Thus, we showed that a unimodal parameter distribution can produce a bimodal period distribution.

Our next step was to determine if electrical coupling between the heterogeneous cells generated by distributing $g_{K(Ca)}$ in the cPBM could account for the robust medium bursting observed in islets (Atwater et al., 1980). For the case of very strong coupling, we were able to calculate the islet behavior without performing further simulations because $g_{K(Ca)}$ appears linearly in the V equation (Eqs. 1 and 6). In such a case, the islet behaves the same as a single cell with the mean value of $g_{K(Ca)}$. To predict the islet behavior, one then just reduces the variance of the $g_{K(Ca)}$ distribution in accordance with the number of cells in the population. (Note that the mean of the islet distribution is shifted to the left compared to the single cell distribution because of the truncation of the Gaussian.) This is illustrated in Fig. 5 for the single-cell distribution represented by curve *D* in Fig. 2, which had given the desired bimodal period distribution for the single cells. However, because the mean of that distribution was in the slow regime, the strongly coupled islet turned out to be slow. In the next paragraph we discuss how with moderate coupling the same distribution could produce almost exclusively medium islets. First, however we note that if distribution *D* of Fig. 2 is shifted to the middle of the medium regime (mean $g_{K(Ca)}$ of 600 pS) the resulting single-cell population consists of only 9.5% medium bursters whereas the islets are predominantly medium (data not shown). Thus, with a period-parameter relationship like the one shown in Fig. 2, it is sufficient to have a broad unimodal distribution of $g_{K(Ca)}$ centered in the medium regime to produce a bimodal single-cell period distribution and medium islets, but it is not necessary if one considers less than perfect coupling.

Intermediate electrical coupling had been shown to prolong the burst period in models incorporating a single slow process (Sherman and Rinzel, 1991). However, Fig. 6 shows that electrical coupling among phantom bursting cells can produce synchronous bursts with periods either longer (see the peak in Fig. 6 near $g_c = 100$ pS) or shorter (see the valley near $g_c = 300$ pS) than a single cell with the population mean value of $g_{K(Ca)}$. The complex mathematical underpinnings of the effects of coupling on islet burst period are best studied in two-cell systems, and are described in detail in a separate manuscript (R. Bertram, C. L. Zimliki, and A. Sherman, unpublished). In brief, the effect of coupling conductance on islet period is determined by the effects of coupling on the action potential characteristics. With weak coupling, the action potentials in neighboring cells are asynchronous, causing them to be reduced in size. Although their amplitude is reduced, the action potentials arise from a more depolarized plateau, which raises the average membrane potential during the active phase. This has two competing consequences: the elevated membrane potential opposes the inhibitory effect of cytosolic Ca^{2+}, requiring calcium to rise to a higher level to terminate the burst. On the other hand, the same elevated membrane potential also allows calcium to rise more rapidly. In models with a single slow variable, as studied to date, the net effect is to the prolong burst period, primarily because it takes longer to clear the increased calcium in the silent phase. In the cPBM, the same holds true for the peak, but at higher coupling strength the reverse occurs, giving rise to the valley. Cytosolic Ca^{2+} rises to still higher levels in the active phase, thereby activating more K(Ca) current. The steep

dependence of $g_{K(Ca)}$ on cytosolic Ca^{2+} may come into play here. A sufficient amount of K(Ca) current is activated to terminate the active phase without need for much contribution by the slower processes, ER filling and increase in ADP/ATP ratio. It is the loss of the participation by these slower processes that accounts for the sharp drop in period, and we therefore conjecture that models with a single slow variable cannot show this effect. As coupling increases further, the action potentials eventually synchronize to the single-cell pattern and the single-cell period is achieved (the plateau at values of $g_c > \sim 400$ pS).

By combining the $g_{K(Ca)}$ distribution of curve *D*, Fig. 2 with a g_c value in the valley, we achieved predominantly medium-oscillating islets without the need to center the distribution in the medium regime of the period-parameter relationship, in contrast to the case with strong coupling. Indeed, in multiple islet simulations, using the $g_{K(Ca)}$ distribution of Fig. 4 *A*, which is centered in the slow regime and produces 67% slow cells, 92.5% of the islets oscillate in the medium regime (Fig. 8, Table 2, line 1). It is interesting to note that the islet burst period distribution itself is bimodal, with both peaks falling in the medium regime. Atwater and colleagues (Atwater et al., 1980) have reported such a distribution for glucose-induced bursting in mouse islets, with peaks at ~15 and 30 s.

Our analysis also reveals that an islet need not contain a minimum number of fast, medium, or slow cells to exhibit a medium emergent oscillation. Groups of cells that are essentially entirely slow (in agreement with many measurements of Ca^{2+} in single β-cells) or entirely fast (in agreement with measurements of electrical activity in single β-cells) can produce medium-oscillating islets, provided that the coupling conductance is chosen correctly (see Fig. 9, and Table 2, lines 2 and 3.) The robustness of the emergent medium oscillation for single-cell distributions giving predominantly fast or slow cells depends on the particular values of μ, σ, and g_c, and appears to be stronger when slow cells predominate. However, our analysis is not meant to favor one particular type of distribution, but rather to underscore the nonobvious and potentially important role for intercellular coupling in shaping the oscillatory behavior of islets.

Although we have emphasized the robustness of medium bursting in islets for a variety of single-cell patterns, the results also show that disparate patterns can be obtained at the single-cell level as a consequence of modest changes in the μ and σ of the populations. The diversity of patterns obtained with the model suggests that the diversity of experimental observations may reflect the intrinsic dynamic range of β-cell oscillation mechanisms combined with subtle differences in experimental technique and/or animal strains.

Our results indicate that changes in the electrical coupling conductance within the islet would have dramatic effects on islet electrical activity. Experimental verification of this prediction is hindered by a lack of selective pharmacological agents to alter cell-to-cell coupling in the islet (Perez-Armendariz et al., 1991). Long-term alteration of gap junction coupling has been achieved through genetic modulation of connexin expression in in vivo and in vitro models (Calabrese et al., 2003; Caton et al., 2003; Le Gurun et al., 2003), but to date insufficient data have been reported to fully evaluate the predictions of the model regarding effects of coupling on burst period. Nevertheless, it is interesting to note that when coupling was enhanced in mouse islets by overexpression of an exogenous gap junction protein (Cx32), glucose-induced bursts and Ca^{2+} oscillations appeared to be slower than in controls (Charollais et al., 2000; Quesada et al., 2003). Conversely, application of the gap junctional blockers heptanol or 18α glycyrrhetinic acid to islet-cell monolayers resulted in a slight decrease in the period (Squires et al., 2000). Intercellular coupling is modulated in cultured islets exposed to high glucose concentrations (Meda et al., 1979), and may contribute at least partially to the favoring of slow oscillations with time in culture (Gilon et al., 1994). Finally, there is also evidence that cell-to-cell electrical coupling within islets changes during the active and silent phases of medium oscillations (Andreu et al., 1997; Mears et al., 1995), but we have not investigated the possible effects of such rapid coupling changes on burst characteristics with our model.

Another strategy for reconciling the differences between single cells and islets was to add stochastic channel noise to models with a single slow variable (Chay and Kang, 1988; Sherman et al., 1988). The cells in these models were all inherently medium oscillators, but channel noise disrupted the activity of single cells, making them appear like fast bursters or continuous spikers. When coupled, the noise was averaged among the cells and the underlying medium oscillation was observed. The model studied here has the benefit of being able to produce a wide range of single-cell burst frequencies and robustly medium-oscillating islets without constraining the average cell to the medium burst regime. However, the model does not exclude that channel noise could also play a role in shaping the behavior of single β-cells. Indeed, the least robust scenario produced by our model is medium islets made up of fast single cells (Fig. 9, *C* and *D*). Preliminary calculations suggest that this scenario is significantly enhanced by inclusion of noise, since noise drives cells that are intrinsically either medium or slow to the fast regime.

One of our goals here was to account simultaneously for the statistical properties of both single cells and islets. We have succeeded to the extent of demonstrating both slow and fast bursting single cells and islets that are predominantly medium bursters. However, other patterns observed in single cells are fast spiking cells, with large amplitude spikes (Falke et al., 1989; Kinard et al., 1999; Zhang et al., 2003) and continuously spiking cells (Gopel et al., 1999b). The model can also account for this class of behavior if one allows heterogeneity in a second parameter, such as g_{Ca}, which

influences spike amplitude and can convert continuous spiking cells into fast bursting cells. This was demonstrated previously using a similar model, which included noise as well (Zhang et al., 2003). However, here we restricted the heterogeneity to a single parameter to keep the analysis simple.

In summary, our analysis shows that the phantom bursting type model, with its inherent fast and slow mechanisms, provides a construct by which diverse distributions of single-cell burst periods can arise in a natural way from unimodal heterogeneity of a single parameter. The single-cell period distributions depend on the mean and standard deviation of the parameter distribution, and tight constraints on these values for medium bursting favor single cell populations that are predominantly fast, predominantly slow, or bimodal with both fast and slow cells. Analysis of the burst properties of islets constructed from cells revealed another property of phantom burst models—that intermediate coupling strength can either prolong or shorten the burst period. The emergent period distribution for diffusely coupled islets therefore depends strongly on the coupling conductance as well as the single-cell parameter distribution, and robustly medium oscillating islets can be constructed from single-cell parameter distributions producing predominantly fast or predominantly slow single cells. Our results motivate further theoretical and experimental study of the role of heterogeneity and cell-to-cell coupling in shaping the burst properties of single β-cells and whole islets.

We thank Netta Cohen for encouraging us to explore comprehensive histograms of period for islets composed of heterogeneous cells.

D.M. acknowledges support from the American Diabetes Association.

REFERENCES

Andreu, E., B. Soria, and J. V. Sanchez-Andres. 1997. Oscillation of gap junction electrical coupling in the mouse pancreatic islets of Langerhans. *J. Physiol. (Lond.).* 498:753–761.

Atwater, I., P. Carroll, and M. Li. 1989. Electrophysiology of the pancreatic β-cell. *In* Molecular and Cellular Biology of Diabetes Mellitus. B. Draznin, S. Melmed, and D. LeRoith, editors. Alan R. Liss, New York. 49–68.

Atwater, I., C. M. Dawson, A. Scott, G. Eddlestone, and E. Rojas. 1980. The nature of the oscillatory behaviour in electrical activity from pancreatic β-cell. *Horm. Metab. Res. Suppl.* 10:100–107.

Atwater, I., L. Rosario, and E. Rojas. 1983. Properties of the Ca-activated K^+ channel in pancreatic β-cells. *Cell Calcium.* 4:451–461.

Bertram, R., J. Previte, A. Sherman, T. A. Kinard, and L. S. Satin. 2000. The phantom burster model for pancreatic β-cells. *Biophys. J.* 79:2880–2892.

Bertram, R., and A. Sherman. 2004. A calcium-based phantom bursting model for pancreatic islets. *Bull. Math. Biol.* In press.

Bertuzzi, F., A. M. Davalli, R. Nano, C. Socci, F. Codazzi, R. Fesce, V. Di Carlo, G. Pozza, and F. Grohovaz. 1999. Mechanisms of coordination of Ca^{2+} signals in pancreatic islet cells. *Diabetes.* 48:1971–1978.

Calabrese, A., M. Zhang, V. Serre-Beinier, D. Caton, C. Mas, L. S. Satin, and P. Meda. 2003. Connexin 36 controls synchronization of Ca^{2+} oscillations and insulin secretion in MIN6 cells. *Diabetes.* 52:417–424.

Caton, D., A. Calabrese, C. Mas, V. Serre-Beinier, A. Charollais, D. Caille, R. Zufferey, D. Trono, and P. Meda. 2003. Lentivirus-mediated transduction of connexin cDNAs shows level- and isoform-specific alterations in insulin secretion of primary pancreatic β-cells. *J. Cell Sci.* 116:2285–2294.

Charollais, A., A. Gjinovci, J. Huarte, J. Bauquis, A. Nadal, F. Martin, E. Andreu, J. V. Sanchez-Andres, A. Calabrese, D. Bosco, B. Soria, C. B. Wollheim, P. L. Herrera, and P. Meda. 2000. Junctional communication of pancreatic β cells contributes to the control of insulin secretion and glucose tolerance. *J. Clin. Invest.* 106:235–243.

Chay, T. R. 1996. Modeling slowly bursting neurons via calcium store and voltage-independent calcium current. *Neural Comput.* 8:951–978.

Chay, T. R. 1997. Effects of extracellular calcium on electrical bursting and intracellular and luminal calcium oscillations in insulin secreting pancreatic β-cells. *Biophys. J.* 73:1673–1688.

Chay, T. R., and H. S. Kang. 1988. Role of single-channel stochastic noise on bursting clusters of pancreatic β-cells. *Biophys. J.* 54:427–435.

de Vries, G., and A. Sherman. 2001. From spikers to bursters via coupling: help from heterogeneity. *Bull. Math. Biol.* 63:371–391.

Dryselius, S., E. Grapengiesser, B. Hellman, and E. Gylfe. 1999. Voltage-dependent entry and generation of slow Ca^{2+} oscillations in glucose-stimulated pancreatic β-cells. *Am. J. Physiol.* 276:E512–E518.

Falke, L. C., K. D. Gillis, D. M. Pressel, and S. Misler. 1989. 'Perforated patch recording' allows long-term monitoring of metabolite-induced electrical activity and voltage-dependent Ca^{2+} currents in pancreatic islet β cells. *FEBS Lett.* 251:167–172.

Gilon, P., J. C. Jonas, and J. C. Henquin. 1994. Culture duration and conditions affect the oscillations of cytoplasmic calcium concentration induced by glucose in mouse pancreatic islets. *Diabetologia.* 37:1007–1014.

Gilon, P., R. M. Shepherd, and J. C. Henquin. 1993. Oscillations of secretion driven by oscillations of cytoplasmic Ca^{2+} as evidences in single pancreatic islets. *J. Biol. Chem.* 268:22265–22268.

Goforth, P. B., R. Bertram, F. A. Khan, M. Zhang, A. Sherman, and L. S. Satin. 2002. Calcium-activated K^+ channels of mouse β-cells are controlled by both store and cytoplasmic Ca^{2+}: experimental and theoretical studies. *J. Gen. Physiol.* 120:307–322.

Gopel, S., T. Kanno, S. Barg, J. Galvanovskis, and P. Rorsman. 1999a. Voltage-gated and resting membrane currents recorded from β-cells in intact mouse pancreatic islets. *J. Physiol.* 521:717–728.

Gopel, S. O., T. Kanno, S. Barg, L. Eliasson, J. Galvanovskis, E. Renstrom, and P. Rorsman. 1999b. Activation of Ca^{2+}-dependent K^+ channels contributes to rhythmic firing of action potentials in mouse pancreatic β cells. *J. Gen. Physiol.* 114:759–770.

Grapengiesser, E., E. Gylfe, and B. Hellman. 1999. Synchronization of glucose-induced Ca^{2+} transients in pancreatic β-cells by a diffusible factor. *Biochem. Biophys. Res. Commun.* 254:436–439.

Gylfe, E., E. Grapengiesser, Y. J. Liu, S. Dryselius, A. Tengholm, and M. Eberhardson. 1998. Generation of glucose-dependent slow oscillations of cytoplasmic Ca^{2+} in individual pancreatic β cells. *Diabetes Metab.* 24:25–29.

Hellman, B., E. Gylfe, E. Grapengiesser, P. E. Lund, and A. Berts. 1992. Cytoplasmic Ca^{2+} oscillations in pancreatic β-cells. *Biochim. Biophys. Acta.* 1113:295–305.

Henquin, J. C., J. C. Jonas, and P. Gilon. 1998. Functional significance of Ca^{2+} oscillations in pancreatic β cells. *Diabetes Metab.* 24:30–36.

Hoel, P. G., S. C. Port, and C. J. Stone. 1971. Continuous random variables. *In* Introduction to Probability Theory. H. Chernoff, editor. Houghton Mifflin, Boston. 109–138.

Jonkers, F. C., and J. C. Henquin. 2001. Measurements of cytoplasmic Ca^{2+} in islet cell clusters show that glucose rapidly recruits β-cells and gradually increases the individual cell response. *Diabetes.* 50:540–550.

Jonkers, F. C., J. C. Jonas, P. Gilon, and J. C. Henquin. 1999. Influence of cell number on the characteristics and synchrony of Ca^{2+} oscillations in clusters of mouse pancreatic islet cells. *J. Physiol. (Lond.).* 520:839–849.

Kanno, T., P. Rorsman, and S. O. Gopel. 2002. Glucose-dependent regulation of rhythmic action potential firing in pancreatic β-cells by K_{ATP}-channel modulation. *J. Physiol.* 545:501–507.

Keizer, J., and G. Magnus. 1989. ATP-sensitive potassium channel and bursting in the pancreatic beta cell. A theoretical study. *Biophys. J.* 56:229–242.

Kinard, T. A., G. de Vries, A. Sherman, and L. S. Satin. 1999. Modulation of the bursting properties of single mouse pancreatic β-cells by artificial conductances. *Biophys. J.* 76:1423–1435.

Larsson, O., H. Kindmark, R. Brandstrom, B. Fredholm, and P. O. Berggren. 1996. Oscillations in K_{ATP} channel activity promote oscillations in cytoplasmic free Ca^{2+} concentration in the pancreatic β cell. *Proc. Natl. Acad. Sci. USA.* 93:5161–5165.

Le Gurun, S., D. Martin, A. Formenton, P. Maechler, D. Caille, G. Waeber, P. Meda, and J. A. Haefliger. 2003. Connexin-36 contributes to control function of insulin-producing cells. *J. Biol. Chem.* 278:37690–37697.

Lenzen, S., M. Lerch, T. Peckmann, and M. Tiedge. 2000. Differential regulation of $[Ca^{2+}]_i$ oscillations in mouse pancreatic islets by glucose, α-ketoisocaproic acid, glyceraldehyde and glycolytic intermediates. *Biochim. Biophys. Acta.* 1523:65–72.

Liu, Y. J., E. Grapengiesser, E. Gylfe, and B. Hellman. 1996. Crosstalk between the cAMP and inositol trisphosphate-signalling pathways in pancreatic β-cells. *Arch. Biochem. Biophys.* 334:295–302.

Liu, Y. J., A. Tengholm, E. Grapengiesser, B. Hellman, and E. Gylfe. 1998. Origin of slow and fast oscillations of Ca^{2+} in mouse pancreatic islets. *J. Physiol. (Lond.).* 508:471–481.

Mears, D., N. F. Sheppard Jr., I. Atwater, and E. Rojas. 1995. Magnitude and modulation of pancreatic β-cell gap junction electrical conductance in situ. *J. Membr. Biol.* 146:163–176.

Meda, P., A. Perrelet, and L. Orci. 1979. Increase of gap junctions between pancreatic B-cells during stimulation of insulin secretion. *J. Cell Biol.* 82:441–448.

Perez-Armendariz, E., and I. Atwater. 1986. Glucose-evoked changes in $[K^+]$ and $[Ca^{2+}]$ in the intercellular spaces of the mouse islet of Langerhans. *Adv. Exp. Med. Biol.* 211:31–51.

Perez-Armendariz, E., I. Atwater, and E. Rojas. 1985. Glucose-induced oscillatory changes in extracellular ionized potassium concentration in mouse islets of Langerhans. *Biophys. J.* 48:741–749.

Perez-Armendariz, M., C. Roy, D. C. Spray, and M. V. Bennett. 1991. Biophysical properties of gap junctions between freshly dispersed pairs of mouse pancreatic β-cells. *Biophys. J.* 59:76–92.

Press, W. H., S. A. Teukolsky, W. T. Vetterling, and B. P. Flannery. 1992. Numerical Recipes in FORTRAN 77: The Art of Scientific Computing. Press Syndicate of the University of Cambridge, New York.

Quesada, I., E. Fuentes, E. Andreu, P. Meda, A. Nadal, and B. Soria. 2003. On-line analysis of gap junctions reveals more efficient electrical than dye coupling between islet cells. *Am. J. Physiol. Endocrinol. Metab.* 284:E980–E987.

Rorsman, P., and G. Trube. 1986. Calcium and delayed potassium currents in mouse pancreatic β-cells under voltage-clamp conditions. *J. Physiol. (Lond.).* 374:531–550.

Santos, R. M., L. M. Rosario, A. Nadal, J. Garcia-Sancho, B. Soria, and M. Valdeolmillos. 1991. Widespread synchronous $[Ca^{2+}]_i$ oscillations due to bursting electrical activity in single pancreatic islets. *Pflugers Arch.* 418:417–422.

Sherman, A., and J. Rinzel. 1991. Model for synchronization of pancreatic β-cells by gap junction coupling. *Biophys. J.* 59:547–559.

Sherman, A., J. Rinzel, and J. Keizer. 1988. Emergence of organized bursting in clusters of pancreatic β-cells by channel sharing. *Biophys. J.* 54:411–425.

Smith, P. A., F. M. Ashcroft, and P. Rorsman. 1990. Simultaneous recordings of glucose dependent electrical activity and ATP-regulated K^+-currents in isolated mouse pancreatic β-cells. *FEBS Lett.* 261:187–190.

Smolen, P., J. Rinzel, and A. Sherman. 1993. Why pancreatic islets burst but single β-cells do not. The heterogeneity hypothesis. *Biophys. J.* 64: 1668–1680.

Squires, P. E., A. C. Hauge-Evans, S. J. Persaud, and P. M. Jones. 2000. Synchronization of Ca^{2+}-signals within insulin-secreting pseudoislets: effects of gap-junctional uncouplers. *Cell Calcium.* 27:287–296.

Zhang, M., P. Goforth, R. Bertram, A. Sherman, and L. Satin. 2003. The Ca^{2+} dynamics of isolated mouse β-cells and islets: implications for mathematical models. *Biophys. J.* 84:2852–2870.

Zimliki, C. L. 2001. Experimental and Theoretical Investigations of the Phantom Bursting Model for Pancreatic Beta-cell Electrical Activity. Johns Hopkins University, Baltimore.